A new bleeding process of additives in a polypropylene film under atmospheric pressure

M. Wakabayashi (a,c), T. Kohno (b), Y. Tanaka (b), T. Kanai (a,c)

(a) Idemitsu Kosan Co., Ltd., Japan
(b) Prime Polymer Co., Ltd., Japan
(c)Graduate School of Natural Science and Technology, Kanazawa University, Japan

Abstract

A new bleeding process of additives in a polypropylene film under atmospheric pressure was investigated. Solubility and diffusion were found to be important for explaining this bleeding process. The experimental results were explained more precisely by assuming two step transport model between the amorphous regions and the crystalline ones. The solubilities and diffusion coefficients of higher fatty acid amides and higher fatty acid such as erucamide (13-cis-docosenamide), behenamide (docosanamide) and behenic acid (docosanoic acid) were determined between 40°C and 70°C. The difference between the solubilities and the diffusion coefficients was discussed with the size of these additives providing aggregates by hydrogen bonding in the polypropylene film. The bleeding profile of erucamide in the ethylene copolymerized polypropylene film was compared with the case in the polypropylene film at 40°C. The solubilities and diffusion coefficients of UV-stabilizers such as 2-(2H-Benzotriazol-2-yl)-4-methylphenol and 2-(2H-Benzotriazol-2-yl)-4-(1,1,3,3-tetramethylbutyl)phenol were determined at 40°C. The difference between the solubilities and the diffusion coefficients were discussed with the solubility parameters and the self diffusion coefficients calculated by using molecular dynamics (MD) simulation.

1 Introduction

Many additives are used to add more favorable qualities to films. There are some additives such as a slip agent or an antistatic additive, etc., that provide performance by bleeding on the surface of the film. Also, there are other additives applied inside the film, for example, a UV-stabilizer and an antioxidant, etc. The bleeding process by which the additive in a film comes to the surface will be considered to be effective in design development of additive prescription, if it can be predicted.

2 Experimental

2.1 Materials

Idemitsu H700 additive-free isotactic polypropylene (iPP) and Idemitsu R740 3.4 wt% ethylene copolymerized polypropylene (Et-co-PP) were used. H700 has a nominal density of 900 kg/m^3, MFR 7.0 g/10min, Tm 163.4°C, ΔHm 101.7J/g, 93.2mol% of isotactic pentad fraction evaluated by ^{13}C NMR spectroscopy and average molecular masses are $M_n = 4.87 \times 10^4$, $M_w = 3.25 \times 10^5$ and $M_z = 1.31 \times 10^6$ estimated by size exclusion chromatography. R740 has a nominal density of 900 kg/m^3, MFR 7.0 g/10min, Tm 139.0°C, ΔHm 79.3J/g and average molecular masses are $M_n = 5.74 \times 10^4$, $M_w = 2.79 \times 10^5$ and $M_z = 1.23 \times 10^6$. Erucamide (13-cis-docosenamide), behenamide (docosanamide) and behenic acid (docosanoic acid) were supplied by NFC Co., Ltd. (Osaka, Japan). 2-(2H-Benzotriazol-2-yl)-4-(1,1,3,3-tetramethylbutyl)phenol (UVA-1, Tinuvin 329) and 2-(2H-Benzotriazol-2-yl)-4-methylphenol (UVA-2, Tinuvin P) were supplied by Ciba-Geigy.

2.2 Sample preparation and measurements

The blends of PP/additive with a small quantity of antioxidant additives (500ppm of IRGANOX 1076 (Ciba-Geigy) and 500ppm of IRGAFOS 168 (Ciba-Geigy)) were prepared by dry mixing and then fed into single-screw extruder operated at 200°C with a screw speed of 100rpm. They were quenched in cold water and cut into the pellet form. The obtained pellets were fabricated into 50 or 60 μm-thick-film using the Φ 40mm T-die casting machine, wherein the temperature from the bottom of the hopper to the T-die was set from 200°C to 230°C with a screw speed of

80rpm. The film was chilled at 30°C. Several sets of 50 sheets of film whose area became 100cm^2 (10cm long and 10cm wide) were prepared and were put in the oven quickly after fabrication for bleeding under the predetermined temperature and time.
A set of the 50 sheets of film was taken out from the oven after predetermined time. Each surface of 50 sheets of film was put in 500ml good solvent such as ethanol, chloroform or acetone for 5 seconds and then washed for 5 seconds. The solvents were eliminated by using rotary evaporator. The amounts of the additives were determined by gas chromatography with Shimadzu GC-14A or size exclusion chromatography with a Waters 410 RI detector.

3 Result and Discussion

3.1 Two step transport model

Figure 1 shows the concept for calculation of the bleeding process[1-3]. The area outside of the film surface is assumed to be the amount of bleeding additive. We considered the bleeding process of the additives under atmospheric pressure as follows. The additive in an iPP film dissolves in an amorphous region first, and if it reaches saturation solubility it becomes impossible to dissolve more. The ingredient beyond this saturation solubility migrates to the film surface at a certain speed according to the diffusion process. Furthermore as shown in Figure 1, it is known that an iPP film has spherulites (S) and amorphous regions (A), which are supposed to have a different contribution to the migration speed in the bleeding process. The spherulites have folded crystalline regions (C) and the additives exist among the crystalline regions (A'). So the model had to be modified in consideration of the amorphous regions and the crystalline regions. We considered that a portion of the excess amount beyond the saturation solubility was restricted within crystalline regions in the spherulites and migrated slowly according to the first-order kinetics. The rest of the excess amount of additives which is not restricted in the crystalline regions exists in the amorphous regions among spherulites. The extent of restriction within crystalline regions was assumed to increase according to the initial amount of the additives. So two step transport model yields the expression

$$y(t) = \left(C_{0,i} - C_s\right)\left\{\alpha_i + \left(1-\alpha_i\right)\left(1-\exp\left(-kt\right)\right)\right\}\left(1 - \frac{1}{4l}\left(\int_{-l}^{l} c(x,t)dx\right)\right) \qquad (1)$$

$$c(x,t) = erf\left(\frac{l-x}{2\sqrt{Dt}}\right) + erf\left(\frac{l+x}{2\sqrt{Dt}}\right) \qquad (2)$$

where $y(t)$ is the amount of bleeding additive on the film surface at time t, $C_{0,i}$ is the i-th initial amount of an additive, C_s is the saturation solubility, α_i is a diffusion ratio of the initial amount $C_{0,i}$, k is the constant of first-order kinetics, l is the half thickness of film, $c(x,t)$ is the concentration at time t and distance x, $erf(x)$ is the error function and D is the diffusion coefficient. The diffusion ratio α_i is assumed to be larger at a lower concentration of additive, because the restriction within the crystalline regions of spherulites is thought to be weak at a lower concentration. Values of α_i, D and C_s are calculated by the least squares technique using a computer program of the best fitting between the experimental data and equations (1) and (2).
The result of behenic acid at 40ºC calculated using the two step transport model is shown in Figure 2. The two step transport model explains the bleeding profile of behenic acid well. The relationship between the saturation solubilities and bleeding temperature and Arrhenius plot are shown in Figure 3 and Figure 4 respectively. As compared with the saturation solubilities and the diffusion coefficients of slip agents at 50°C, both saturation solubility and diffusion coefficient of behenic acid are larger than those values of erucamide, and both values of behenamide are smallest. The molar masses of behenic acid (MW:341), behenamide (MW:340) and erucamide (MW:338) are almost the same. Then it is thought that the molecular size of behenic acid is smaller than that of erucamide and the molecular size of erucamide is smaller than that of behenamide. The reason why there are big differences between the saturation solubilites and the diffusion coefficients of slip agents is thought to be because the self-

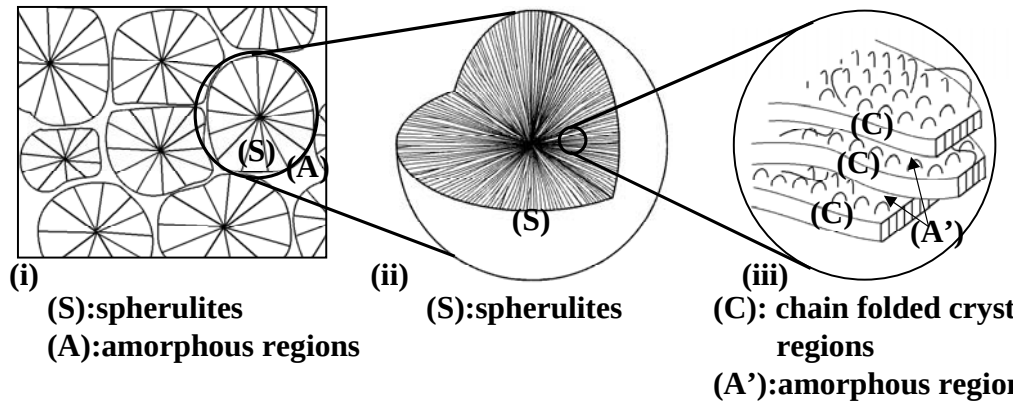

Figure 1: Internal structure of isotactic polypropylene:
(i) spherulites (S) and amorphous regions (A) among spherulites in iPP film
(ii) internal structure of a spherulite(S)
(iii) the chain folded crystalline regions (C) and amorphous regions (A') among the chain folded crystalline regions.

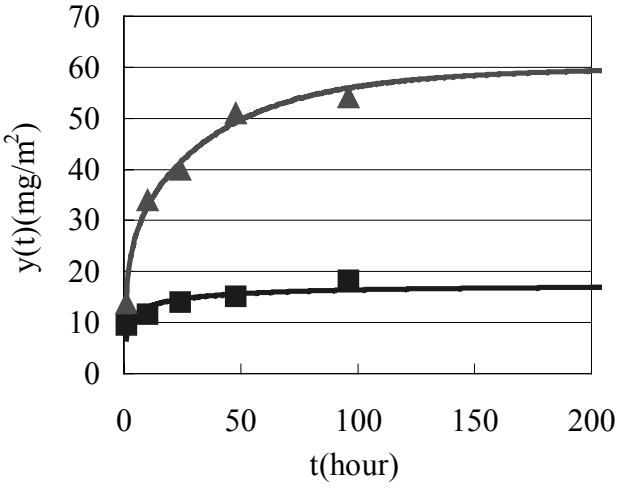

Figure 2: Bleeding profiles of behenic acid at 50ºC. Initial amount ($C_{0,i}$) : $C_{0,1}$ = 5,000ppm (■); $C_{0,2}$ = 7,000ppm (▲). The full lines are calculated by using the two step transport model.

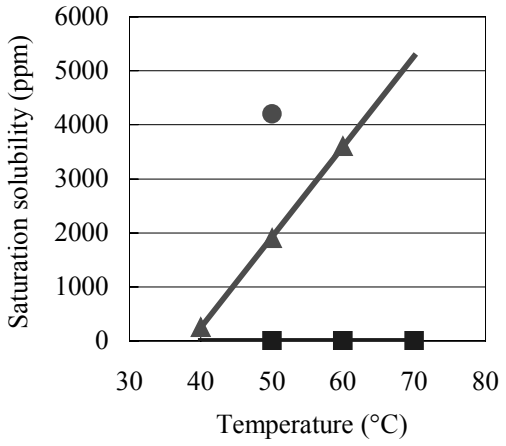

Figure 3: Saturation solubility against T
behenic acid(●); erucamide (▲); behenamide (■)

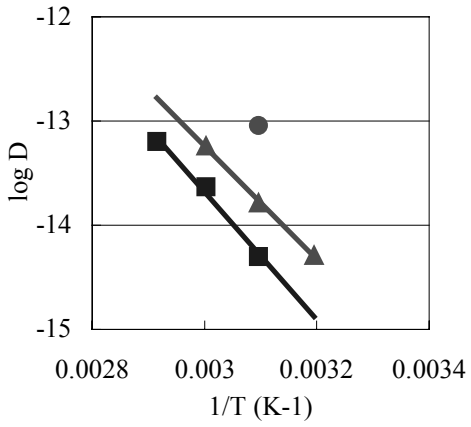

Figure 4: Arrhenius plot as ln D against 1/T
behenic acid(●); erucamide (▲); behenamide (■)

association of erucamide and behenamide by hydrogen bonding occurs in iPP film and the size of the aggregates influences both saturation solubilities and the diffusion coefficients of slip agents.

The result of erucamide in Et-co-PP film at 40ºC calculated using the two step transport model is shown in Figure 5. The two step transport model explains the bleeding profile well. The relationship between the saturation solubilities and bleeding temperature and Arrhenius plot are shown in Figure 6 and Figure 7 respectively. As compared with the saturation solubilities and the diffusion coefficients of erucamide at 40°C, the saturation solubility of erucamide in ET-co-PP film was almost the same as that of erucamide in iPP film but the diffusion coefficient of erucamide in ET-co-PP film was slightly smaller than that of erucamide in iPP film. This shows that in spite of low crystallinity the saturation solubility in ET-co-PP was not influenced by the crystallinity and the diffusion coefficient in ET-co-PP decreased. It would seem that the interaction between the polymer and the erucamide is significant rather than the crystallinity.

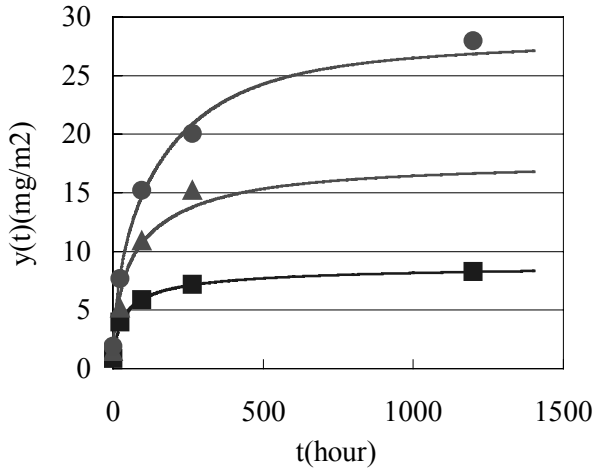

Figure 5: Bleeding profiles of erucamide in ET-co-PP film at 40ºC. Initial amount ($C_{0,i}$) : $C_{0,1}$ = 500ppm (■); $C_{0,2}$ = 900ppm (▲); $C_{0,3}$ = 1,400ppm (●). The full lines are calculated by using the two step transport model.

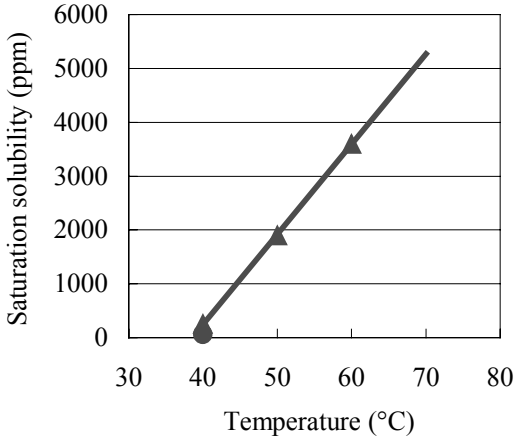

Figure 6: Saturation solubility against T R740(●); H700 (▲)

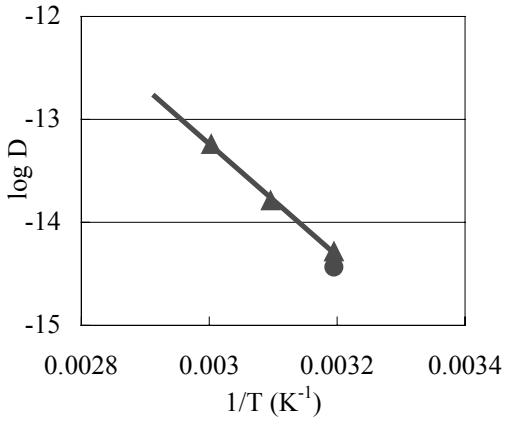

Figure 7: Arrhenius plot as ln D against 1/T R740(●); H700 (▲)

3.2 Estimation by molecular dynamics (MD)

Table 1 shows the parameters of UV-stabilizers obtained from two step transport model. In order to study the cause in which UV-stabilizers with the almost same structures have a big difference in bleeding process, the important factors C_s and D were examined using molecular dynamics (MD). The MD simulations were performed using commercial package, NanoBox software from Nano Simulation Associates, Japan[4-6]. The Hildebrand solubility parameter (δ) is defined as the square root of cohesive energy density

$$\delta = \sqrt{\frac{E_{coh}}{V}} = \sqrt{\frac{E_{vac} - E_{bulk}}{V}} \tag{3}$$

where E_{coh} is the cohesive energy per mole, E_{vac} is the potential energy in the vacuum state, E_{bulk} is the potential energy in the bulk state and V is the mole volume. The values of E_{vac}, E_{bulk} and V were calculated from MD simulation. The solubility parameters of UVA-1 and UVA-2 obtained by MD calculation are 19.3, 22.7 respectively. As compared with these solubility parameters, the solubility parameter of UVA-1 is closer to that of PP (δ=17.2[8]). This result is consistent with the fact that the saturation solubility of UVA-1 becomes larger than that of UVA-2. It is supposed that the solubility parameter influences the saturation solubility because of the different compatibility of the functional group.

The values of the diffusion coefficients obtained by this two step transport model were compared with the result of MD simulation. The self diffusion coefficients (D_{self}) were calculated using the equation below

$$D_{self} = \lim_{t\to\infty} \frac{1}{6t} \left\langle \left| \mathbf{r}(t+t_0) - \mathbf{r}(t_0) \right|^2 \right\rangle \tag{4}$$

where $\left\langle \left| \mathbf{r}(t+t_0) - \mathbf{r}(t_0) \right|^2 \right\rangle$ is the averaged mean square distribution, $\mathbf{r}(t)$ is the center of gravity of the additive. The values of D_{self} were calculated using data from 60ps to 200ps. Figure 8 shows the time dependency of the mean square distribution of UVA-1 and UVA-2. Figure 9 shows the comparison between the self diffusion coefficients calculated from MD and the diffusion coefficients obtained from the two step transport model. There are good relationship between the diffusion coefficients from MD and the two step transport model. Since UVA-1 has a large functional group (tert-octyl group), it is thought that the diffusion coefficient of UVA-1 is smaller than that of UVA-2. The values of the self diffusion coefficients of both UV-stabilizers from MD are quite smaller than the value of methane (0.7-1.3 × 10^{-10}m^2/s)[7], however these values are still about 100 times as large as the diffusion coefficients obtained from the two step transport model. The calculated values from MD present the self diffusion coefficients of additives of Brownian motion in the very narrow range (about 2Å) of the amorphous state. On the other hand, the calculated values from the two step transport model present relative diffusion

Table 1: Parameters of UV-stabilizers obtained from two step transport model

Additive	Temperature °C	Saturation Solubility Cs, ppm	Diffusion coefficient D, m2/s	Constant offirst-order kinetics k, 1/s	Diffusion ratio		
					α_1	α_2	α_3
UVA-1	40	13,000	2.4 × 10^{-14}	8.1 × 10^{-7}	0.0[a]	0.0[a]	0.0[a]
UVA-2	40	3,000	7.4 × 10^{-14}	1.4 × 10^{-5}	0.11[b]	0.11[b]	

the initial amounts of additives ($C_{0,i}$)

[a] $C_{0,1}$:15,000ppm, $C_{0,2}$:17,500ppm, $C_{0,3}$:20,000ppm

[b] $C_{0,1}$: 4,300ppm, $C_{0,2}$:6,300ppm

coefficients of UV-stabilizers which are thought to be restricted by the various barriers when the additives pass from the crystalline regions to the amorphous regions among the spherulites and pass through the amorphous regions to the film surface as shown in Figure 1.
It is demonstrated that the MD simulation is useful for predicting the saturation solubilities and the diffusion coefficients of UV-stabilizers qualitatively in spite of the large molecular sizes and complex structures of iPP film.

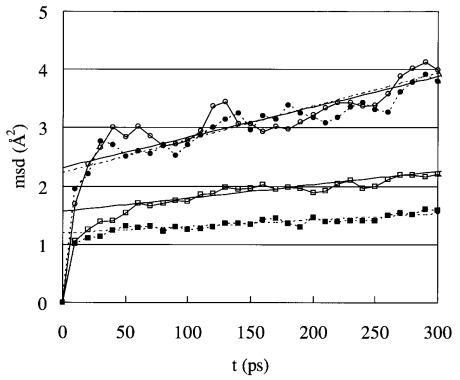

Figure 8: Mean square distribution of UV-stabilizers as a function of time; Tinuvin 329: (□, ■); Tinuvin P: (○, ●). The straight lines shows the least-squares fit by using data from 60 to 200ps.

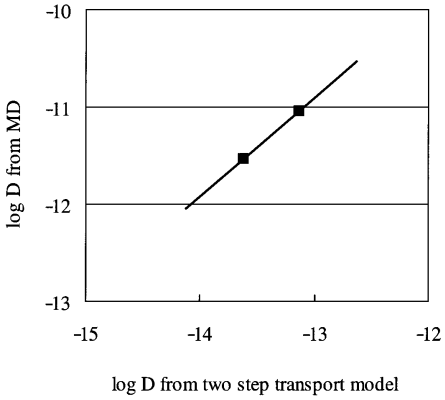

Figure 9: Comparison of the self diffusion coefficients from MD with the relative diffusion coefficients from two step transport model.

4. Conclusion

A new bleeding model of additives in polypropylene film under atmospheric pressure was investigated. The two step transport model explains the bleeding profiles of slip agents and UV-stabilizers well. By using this model, the saturation solubilities and diffusion coefficients of the slip agents and UV-stabilizers were directly determined between 40°C and 70°C. The differences between the saturation solubilites and the diffusion coefficients of slip agents can be explained by assuming that the self association of erucamide and behenamide by hydrogen bonding occurs in iPP film. As compared with the saturation solubilities and the diffusion coefficients of erucamide in ET-co-PP film and iPP film at 40°C, It would seem that the interaction between the polymer and the erucamide is significant rather than the crystallinity. By using MD simulation, the Hildebrand solubility parameter is supposed to influence the saturation solubility because of the different compatibility of the functional group. The size of the functional group is also supposed to influence the diffusion coefficient. MD simulation is useful for predicting the saturation solubilities and the diffusion coefficients qualitatively in spite of the large molecular sizes and complex structures of iPP film.

5. References

1. Wakabayashi, M.; Kohno, T.; Kimura, T.; Tamura, S.; Endoh, M.; Ohnishi, S.; Nishioka, T.; Tanaka, Y.; Kanai, T. J Appl Polym Sci 2007, 104, 3751.
2. Wakabayashi, M.; Kohno, T.; Kimura, T.; Tamura, S.; Endoh, M.; Ohnishi, S.; Nishioka, T.; Tanaka, Y.; Kanai, T. to be accepted for publication.
3. Wakabayashi, M.; Kohno, T.; Kimura, T.; Tamura, S.; Endoh, M.; Ohnishi, S.; Nishioka, T.; Tanaka, Y.; Kanai, T. 22nd Annual Meeting of the Polymer Processing Society, 2006.
4. Kuwajima, S.; Manabe, A. Chem. Phys. Lett. 2000, 332, 105.
5. Kikuchi, H.; Kuwajima, S.; Fukuda, M. J Chem Phys 2001, 115, 6258.
6. Kuwajima, S.; Kikuchi, H.; Fukuda, M. J Chem Phys 2006, 124, 124111.
7. Fukuda, M.; Kuwajima, S. J Chem Phys 1998, 108, 3001.
8. Matsuura, T.; Blais, P.; Sourirajan, S. J Appl Polym Sci 1976, 20, 1515.